Available online at www.CivileJournal.org

Civil Engineering Journal

(E-ISSN: 2476-3055; ISSN: 2676-6957)

Vol. 7, No. 10, October, 2021

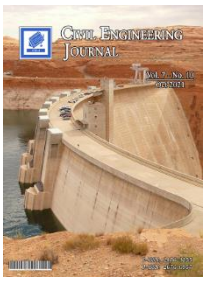

Study of Pressure Distribution on an Irregular Octagonal Plan Oval-Shape Building Using CFD

Arun Kumar [1], Ritu Raj [1*]

[1] *Research Scholar, Department of Civil Engineering, Delhi Technological University, Delhi, India.*

[2] *Assistant Professor, Department of Civil Engineering, Delhi Technological University, Delhi, India.*

Received 03 August 2021; Revised 16 September 2021; Accepted 23 September 2021; Published 01 October 2021

Abstract

This paper aims to study the wind flow characteristics and to analyze the wind pressure distribution on the surfaces around an irregular octagonal plan shape building model. There is a central open space in plan to provide more surface area around the building for natural ventilation. Plan area of the building is 300 m^2 (excluding the open space) and height is 50 m. Steady state flow of wind with 5% turbulence (moderate turbulence) under atmospheric boundary layer has been taken in the study. Numerical simulation with standard k-ε model using ANSYS (CFX) software has been used for the purpose. Flow characteristics has been studied in terms of flow separation, reattachment of flow, creation of wakes and vortices. The surface pressure generated around the model has been studied in terms of coefficient of pressure. The model is symmetrical about both the axes in plan. Hence, study for different wind angle of attacks from 0° to 90° @ 30° interval has been conducted. The flow characteristics and unusual or critical coefficient of pressure on surfaces of the model observed have been discussed.

Keywords: Oval plan-Shape Building; ANSYS (CFX); Wind Pressure Coefficient; k-ε model.

1. Introduction

Wind pressure is an important factor governing the natural ventilation, pedestrian comfort and design of tall buildings. Computational Fluid Dynamics (CFD) modelling is a convenient, economic and faster solution to access the wind pressure in tall buildings of various architectural shapes specially during the preliminary stage of finalization of any project. Through numerical simulation, wind response on tall buildings for structural variables like moments, loads, pressure etc. can be calculated up to a level of acceptable accuracy. For understanding the natural ventilation in buildings wind pressure is the primary characteristic whereas the force and moment it exerts on structure may be utilized for structural resistance and stability. ANSYS (CFX) is one of the numerical simulation tools that is used for analysing the wind pressure on tall buildings. In ANSYS (CFX) complex geometry of buildings can be easily modelled and discretization of geometry into smaller elements for numerical analysis with good quality meshing can be achieved with full control. Changes in the geometry and meshing can also be easily done for parametric studies.

Wind flow is a complex phenomenon and it has a typical behavior to exert differential velocity and pressure around any bluff body coming in its way of flow direction. Though, for ease in analysis a time averaged steady state of uniform flow condition is taken, wind does not flow with a uniform speed and in a constant direction. Wind speed

* Corresponding author: rituraj@dtu.ac.in

http://dx.doi.org/10.28991/cej-2021-03091760

© 2021 by the authors. Licensee C.E.J, Tehran, Iran. This article is an open access article distributed under the terms and conditions of the Creative Commons Attribution (CC-BY) license (http://creativecommons.org/licenses/by/4.0/).

consists of series of turbulences in the form of gusts which vary both in magnitude and direction very widely. Even the phenomenon of uniform and steady wind is not that much simple. The load produced by the wind depends upon the form of the structure too. It becomes more relevant with the increase in height of the structure due to atmospheric boundary layer effect (ABL) and in high rise buildings due to cantilever effect with fixed end at the ground. It has been observed that above the height of 62 m, the height factor is so pronounced that the effect of wind becomes more prominent than the seismic effect while considering the horizontal load on the building [1].

When wind is at rest, the normal atmospheric pressure is acting all around any structure and the load on the structure is balanced in totality. As the wind starts its motion, at some point on the obstacle there is increase in pressure and at others decrease in pressure. The magnitude of these changes is usually less than 2 % of the normal pressure. These change in pressure distribution on the structure are converted into a single load/force as a resultant of them during the analysis of the structure. The maximum increase in pressure produced by the wind is, where is the density of air and the wind speed encountered by the obstacle/structure. This is termed as velocity pressure or impact pressure. The change in pressure differences is generally expressed as a dimensionless coefficient of pressure (C_{pe}) which is ratio of the pressure difference to the velocity pressure represented as:

$$C_{Pe} = \frac{\Delta P}{\rho u^2/2} \quad (1)$$

where, $\Delta P = P - P_o$, P being pressure at any point and P_o the reference pressure (atmospheric pressure in natural wind condition), is density of air and , the uniform velocity field.

In a boundary layer flow where gradient velocity field exists, it is not so simple to define the uniform velocity field. As such, is chosen at a reference height or velocity at the level at which the pressure is measured. All values in the present study have been worked out based on the velocity at the level of the roof top of the model where velocity is found to be maximum. In this way points corresponding to the maximum can be identified where wind pressure is maximum. Although the maximum increase in pressure at any point is equal to the velocity pressure, the fluctuating wind produces pressure decrease of greater amount at any point on the surface and hence the average wind pressure resulting from the surface distribution over an area becomes greater than the velocity pressure. The coefficient thus obtained is independent of the wind speed and scale of the model. However, it is influenced by form of the structure, size of the structure, direction of the wind, terrain characteristic and location of surrounding structures. Various international codes for design of structure have provided values but, the available data are for regular plan shapes in orthogonal directions only. Structural design of structure based on these data increases the cost of construction. As such, experiments must be performed for every individual structure to appropriately investigate the wind stresses to incorporate it in the structural design. Baines (1952) [2] firstly depicted the effect of velocity distribution due to wind and its flow pattern on tall buildings. The contour of the mean wind pressure was intuitively demonstrated as positive pressure on upwind side and negative pressures on sides, top and back surfaces of a square shaped building. Various research papers in the field of wind engineering on different shape of high-rise buildings have been published by researchers.

Gomes et al. (2005) [3] investigated wind pressure distribution on the faces of 'L' and 'U' plan shape tall buildings by using Wind Tunnel Test as well as Computational Fluid Dynamics (CFD) models. Mohotti et al. (2014) [4] studied the interference effect as well as along wind & across wind effects for tall buildings using Wind Tunnel Tests and CFD. Zhao & Lam (2008) [5] investigated the interference effects between five square tall buildings arranged in L-shape and T- shape pattern, arranging them in in the wind tunnel testing. It was found that strong interference effect does exist on all member buildings. The wind loads were significantly modified due to the interference effect as compared to the single isolated buildings. Amin & Ahuja (2011) [6] studied wind induced pressure on buildings of various geometries. Tanaka et al. (2012) [7] presented aerodynamic characteristics of different irregular plan shaped tall buildings by wind tunnel tests. Amin & Ahuja (2013) [8] investigated the effect of different side ratios on a rectangular building model of same plan area and height. Chakraborty and Dalui (2013) [9] presented a paper on numerical study of pressure distribution on different faces of square plan shaped tall buildings under 0°, 30° and 45° wind angles using ANSYS (Fluent). Bhattacharyya et al. (2014) [10] studied pressure distribution of various faces of 'E' plan shaped tall building through physical and analytical wind tunnel for various wind angles. Kheyari and Dalui (2015) [11] have studied the wind load on a tall building under interference effects through CFD. Roy and Bairagi (2016) [12] studied wind pressure and velocity pattern around stepped tall building comprising of rectangular, square and triangular shape placed one above each other. Study of wind pressure and velocity pattern around 'N' plan shaped tall building was conducted by Mukherjee and Bairagi (2017) [13].

Bairagi & Dalui (2020) [14] studied the pressure distribution of square tall building with 20% setback at h/2 and 10 % setback each at h/3 and 2h/3. Pal and Raj (2021) [15] studied the effect of interference of square plan shape and remodel triangular shape building having same plan area for 100 % blockage condition. It has been revealed that model geometry and orientation of duplicate building models have a significant role on pressure and force generated on the principal building. Raj and Ahuja (2013) [16] studied rigid model tall buildings of same plan area on square and

plus shape having varying wing lengths through open circuit boundary layer experiments and reported that the base shear, base moments and twisting moments depends not only on wind directions but also on cross sectional shapes. Raj et al. (2020)[17] studied numerical simulation of ANSYS (CFX) on H plan shaped tall buildings under isolated and interference conditions by similar plan shape model at different locations. Pal et al. (2021) [18] have reported their comparative study conducted through open wind tunnel test for wind induced mutual interference on twin square and fish plan shape tall buildings placed at a distance of 10% height of building with different combination of orientation between front and back. They have reported induced pressure and base shear in their study. Nagar et al. (2020) [19] studied pressure coefficient and IF for different interference conditions of square and H plan shaped tall buildings having same plan area and reported that H plan shape is subjected to higher pressure than the square model. Proximity effects on an existing target tall building due to proposed super tall building with a pair of similar buildings adjacent to the target building has been studied by Quan et al. (2020) [20]. It was reported that the aerodynamic response of the target building increased considerably when the proposed super building exists in the flow direction upstream the target building.

In this paper a brief description is being presented to understand the wind flow characteristics under atmospheric boundary layer (ABL) condition and the surface pressure distribution on the surfaces of an irregular octagonal plan oval-shaped building of height 50 m and plan area 300 m^2 (Figure 1) with a central opening and to evaluate values on the faces through ANSYS (CFX). Standard k-ε model for simulation has been used for the analysis.

Information about wind environmental analysis on irregular plan shaped building model with a central vertical opening duct is not available in literature. The central opening provides more surface area around the building. This will improve natural ventilation and allow more sun light inside the building leading to energy saving for thermal comfort and better lighting. Variation of pressure distribution on the faces for varied wind incident angles studied in the present study is useful for designing cladding units on the surfaces of such buildings for safety under wind loads.

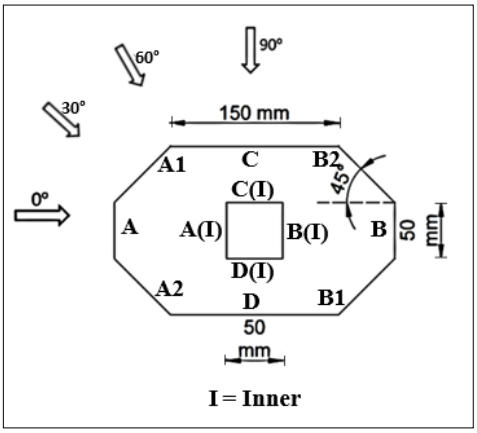

Figure 1. Oval Plan-Shape Model

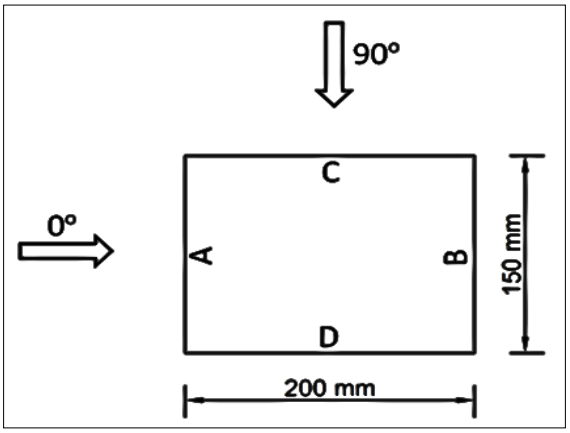

Figure 2. Rectangular Plan-Shape Model

2. Research Methodology

The flowchart (Figure 3) shows the systematic procedure of numerical study carried out with model of rectangular building (Figure 2) having plan area (300 m^2) and height (50 m) as that of the irregular octagonal building under study. It is done to validate the results by comparing the values with different code of practices (Table 1). The same CFX parameters was applied for study of irregular octagonal plan shape model. Other plan shape models have also been studied but they are beyond the scope of this paper.

3. Validation

The validity of the numerical approach studied was done by simulating a rectangular plan shape model (Figure 2) of same plan area and height as that of the octagonal plan oval-shaped model in the same wind flow and boundary conditions. The results of the coefficient of pressure on the faces of the rectangular model were compared with different international code of practices (Table 1) and found to be within acceptable limit, especially for the windward and leeward wind faces. Some larger differences are apparent on the side faces due to three-dimensional unsteady nature of turbulence and eddy viscosity of flow. However, the numerical simulation has captured the main flow characteristics discussed later on and supports the reasonability of the approach for further study on octagonal plan oval-shaped model.

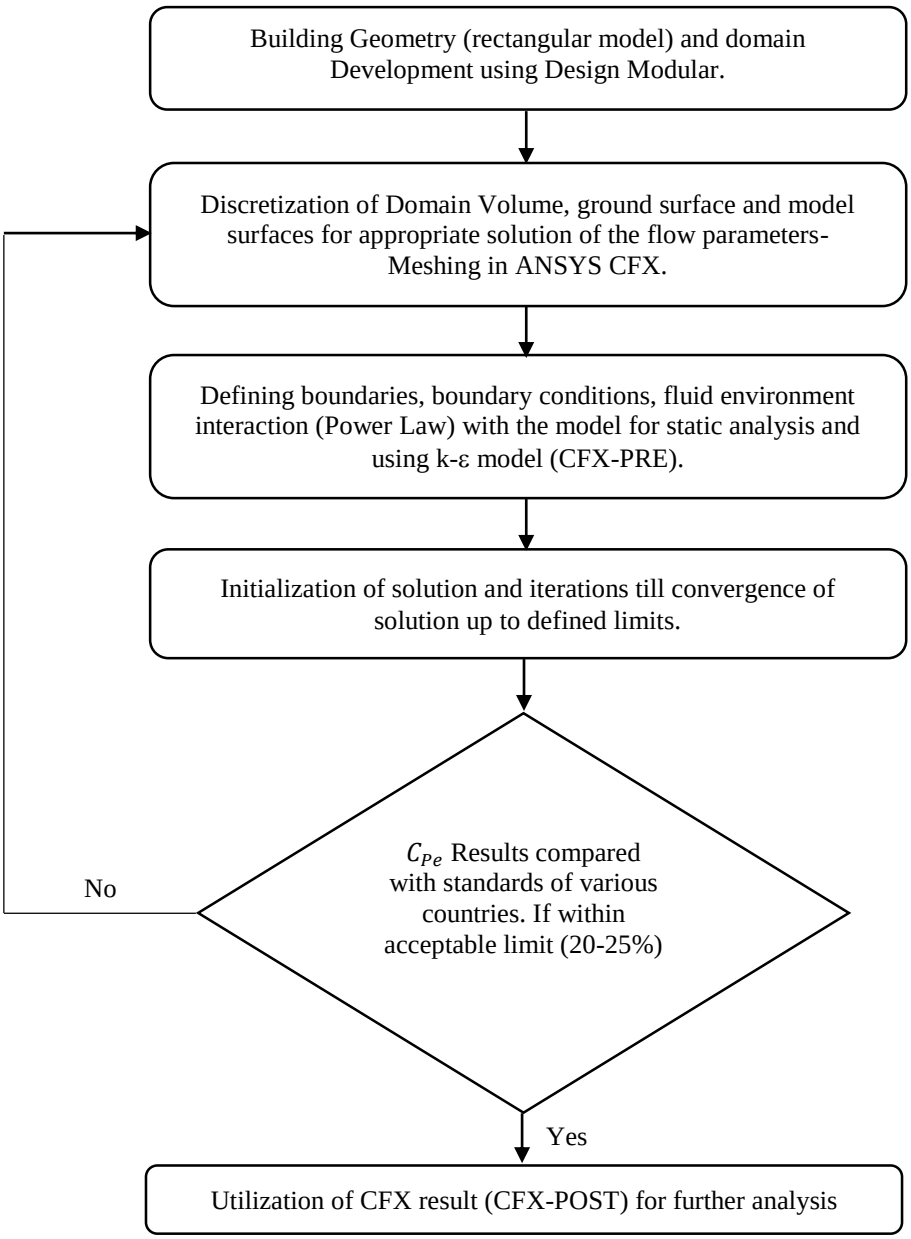

Figure 3. Flow Chart of ANAYS CFX Simulation of Model

Table 1. Comparison of on Faces of Rectangular Model

As per	Wind Angle	C_{Pe} Face A (Windward Face)	C_{Pe} Face B (Leeward Face)	C_{Pe} Face C (Side Face)	C_{Pe} Face D (Side Face)
ANSYX (CFX)	0˚	+ 0.71	- 0.23	- 0.44	- 0.43
	90˚	- 0.48	-0.48	+ 0.68	- 0.28
IS: 875 (Part 3): 2015	0˚	+ 0.8	- 0.25	- 0.8	- 0.8
	90˚	- 0.8	- 0.8	+ 0.8	- 0.25
ASCE/SEI 7-10	0˚	+ 0.8	- 0.5	- 0.7	- 0.7
	90˚	- 0.7	- 0.7	+ 0.8	- 0.5
AS/NZS- 1170.2 (2002)	0˚	+ 0.8	- 0.5	- 0.65	- 0.65
	90˚	- 0.65	- 0.65	+ 0.8	- 0.5
EN: 1991-1-4	0˚	+ 0.8	- 0.55	- 0.8	- 0.8
	90˚	- 0.8	- 0.8	+ 0.8	- 0.55
BS: 6399-2	0˚	+ 0.76	- 0.5	- 0.8	- 0.8
	90˚	- 0.8	- 0.8	+ 0.76	- 0.5

4. Numerical Analysis

Three-dimensional unsteady flow of any fluid is defined by the Navier-Stokes Equations of Continuity and Momentum. The velocity and pressure in the fluid flow environment is governed by them. Computational Fluid Dynamics (CFD) models attempt to resolve the flow of the fluid around any bluff body by simulating the flow at finite grid locations. Based on the continuity and momentum equations various mathematical models, researchers have developed, to know the flow characteristics and the effect of turbulence in a fluid flow. Different models have been developed to match the near real scenario occurring in the nature. However, no model has been developed so far to know the exact turbulence flow characteristics. Among them k- epsilon (k-ε) model is the most commonly used model in CFD simulation for environmental wind flow conditions. The exact k-ε model equation contains many variables and unknowns which are unmeasurable. In the standard k-ε model applied in the present study using ANSYS (CFX) software description of turbulence is defined by two transport equations in partial differential form. The first transport equation is in terms of the variable 'Turbulence Kinetic Energy (k)' and the second equation is in terms of the variable 'Dissipation of Turbulence Kinetic Energy (ε)'. It is the simplest model for which only initial and/or boundary conditions needs to be supplied. Turbulence Kinetic Energy (TKE) is produced by shear, friction or buoyancy or by small eddies developed by fluid flow. It is the mean kinetic energy per unit mass associated with eddies in turbulent flow having dimension of $[L^2T^2]$. Physically, the TKE is characterized by root mean square (RMS) velocity fluctuations. TKE is transferred into turbulence energy which is dissipated, (turbulent eddy dissipation, ε), by viscous forces at microscale (Kolmogorov scale) producing heat. ε has the dimension of $[L^2T^3]$ i.e., turbulent kinetic energy per unit time. In ANSYS (CFX) [21] the Navier-Stokes equations of continuity and momentum for fluid flow and the differential transport equations of turbulent kinetic energy and turbulent eddy dissipation have been taken as in Equations 2 to 9 [4].

Continuity Equation

$$\frac{\partial \rho}{\partial t} + \frac{\partial}{\partial x_j}\left(\rho U_j\right) = 0 \tag{2}$$

Momentum Equation

$$\frac{\partial \rho U_i}{\partial t} + \frac{\partial}{\partial x_j}\left(\rho U_i U_j\right) = -\frac{\partial p'}{\partial x_i} + \frac{\partial}{\partial x_j}\left[\mu_{eff}\left(\frac{\partial U_i}{\partial x_j} + \frac{\partial U_j}{\partial x_i}\right)\right] + S_M \tag{3}$$

Where S_M is sum of body forces, μ_{eff} is effective viscosity accounting for turbulence and p' is the modified pressure defined as below. Rest symbols are carrying usual meanings.

$$p' = p + \frac{2}{3}pk + \frac{2}{3}\mu_{eff}\frac{\partial U_k}{\partial x_k} \tag{4}$$

$$\mu_{eff} = \mu + \mu_t \tag{5}$$

where μ_t is the turbulent viscosity which is linked to the turbulence kinetic energy and dissipation by the flowing equation:

$$\mu_t = C_\mu \rho \frac{k^2}{\varepsilon} \tag{6}$$

where $C_\mu = 0.09$, a constant called k-ε turbulence model constant.

On the basis of differential transport equations of continuity and momentum above, turbulence kinetic energy and rate of turbulence eddy dissipation are expressed respectively as:

Turbulent Kinetic Energy Equation:

$$\frac{\partial(\rho k)}{\partial t} + \frac{\partial}{\partial x_j}\left(\rho U_j k\right) = \frac{\partial}{\partial x_j}\left[\left(\mu + \frac{\mu_t}{\sigma_k}\right)\frac{\partial k}{\partial x_j}\right] + P_k - \rho\varepsilon + P_{kb} \tag{7}$$

Turbulent Eddy Dissipation Equation:

$$\frac{\partial(\rho\varepsilon)}{\partial t} + \frac{\partial}{\partial x_j}\left(\rho U_j \varepsilon\right) = \frac{\partial}{\partial x_j}\left[\left(\mu + \frac{\mu_t}{\sigma_\varepsilon}\right)\frac{\partial \varepsilon}{\partial x_j}\right] + \frac{\varepsilon}{k}\left(C_{\varepsilon 1}P_k - C_{\varepsilon 2}\rho\varepsilon + C_{\varepsilon 1}P_{\varepsilon b}\right) \tag{8}$$

where, $C_{\varepsilon 1}, C_{\varepsilon 2}, \sigma_k$ and σ_ε are k-ε turbulent model constants, the values of whom have been arrived after numerous iterations of data fitting for a wide range of turbulence flows as:

$C_{\varepsilon 1}$ = 1.44, $C_{\varepsilon 2}$ = 1.92, σ_k = 1.0 and, σ_ε = 1.3

P_k is turbulence production due to viscous forces and P_{kb} & $P_{\varepsilon b}$ represents the buoyancy production term. For incompressible flow,

$$P_k = \mu_t\left(\frac{\partial U_i}{\partial x_j} + \frac{\partial U_j}{\partial x_i}\right)\frac{\partial U_i}{\partial x_j} \tag{9}$$

5. Mean Velocity Characteristics

In nature wind does not flow uniformly. In the ABL profile, speed of wind increases as height from earth increases due to lesser friction exerted by roughness created by vegetation and structures at ground. As such, in high rise building the wind flow encountered is not uniform across the height of the building. The governing empirical equations of ABL wind flow are:

(1) Parabolic Law:

$$u = u_{Ref}\sqrt{\frac{Z+22}{Z_{Ref}+22}} \tag{10}$$

where, u_{Ref} = Reference Wind Speed in m/s; Z_{Ref} = Reference height 10 m; and u = Time averaged longitudinal velocity at heigh Z above ground.

(2) Power Law:

$$u = u_{Ref}\left(\frac{Z}{Z_{Ref}}\right)^{\alpha} \tag{11}$$

where, α is a function of terrain roughness.

While power Law is an improvement in the Parabolic Law, it is not analytically correct for the bottom 10 m of ABL. Still, it is widely used for its simplicity.

(3) Logarithmic Law:

$$u = \frac{1}{k}u_0 L_n\left(\frac{Z-Z_d}{Z_0}\right) \tag{12}$$

Where, k = 0.4 (Von Karman Constant); u_0 = Friction Velocity; $u_0 = \sqrt{\frac{\tau_w}{\rho}}$; τ_w = Wall Shear Stress = $\mu\left(\frac{du}{dy}\right)_{y=0}$ and ρ = Density of Air; Z_0 = Aerodynamic roughness length; Z_d = Zero plane displacement.

Logarithmic Law is applicable to lower 10 m height from the ground.

6. Model and Computational Domain

In the present study the building model is placed within the domain, which is analogous to a wind tunnel. Domain size is selected such that its boundaries are not affected by the model placed in it or in other words the computational domain is kept large enough to avoid reflection of fluid streams to avoid

Abnormal fluid pressure field around the model and also to keep the blockage ratio less than 3%. At the same time velocity fluctuations, uplift force and backwash, vortex generation in the wake region etc. should be effectively created during the simulation. Recommendations of Revuz et al. (2012) [22] in the matter have been adopted in the present study. The domain size should also not be large otherwise it will require a larger number of computational cells for analysis which needs more time and higher computational facility for the solution to converge. The size of the computational domain in the flow direction and the side domain walls are kept equal to 5H each from the respective faces of the model, H being the height of the model. The distance behind the model is kept as 15H so that proper wake and vortex is generated behind the model. The height of the domain above the domain floor is kept as 6H. In the present study the domain of size L =10.3 m, B = 5.3 m and H = 3.0 m with the model (1:100 scale) kept within from the respective domain boundaries are taken as shown in Figure 4. Steady state wind flow under ABL for terrain category-II [6] at the inlet using the power law index as 0.143 and with 5% turbulence intensity (to provide the gustiness effect) has been adopted. Reference velocity equal to 0.63 m/s at the roof height of the model has been provided. The velocity profile at inlet achieved is shown in Figure 5.

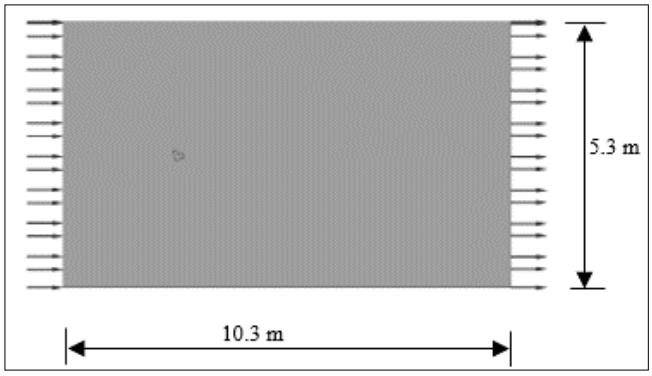

(a) Plan

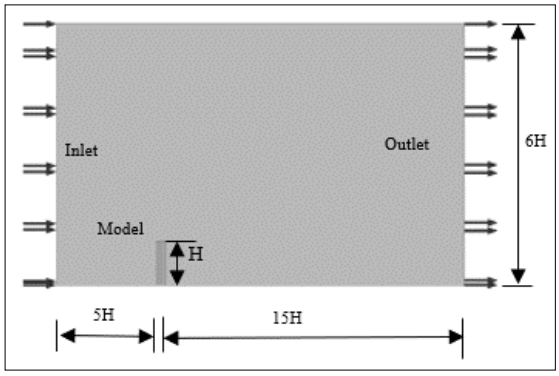

(b) Elevation

Figure 4. Schemetic Diagram of Domain

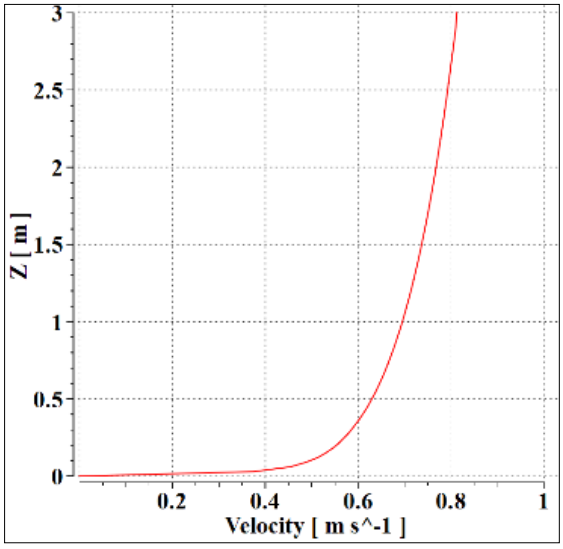

Figure 5. Velocity Profile

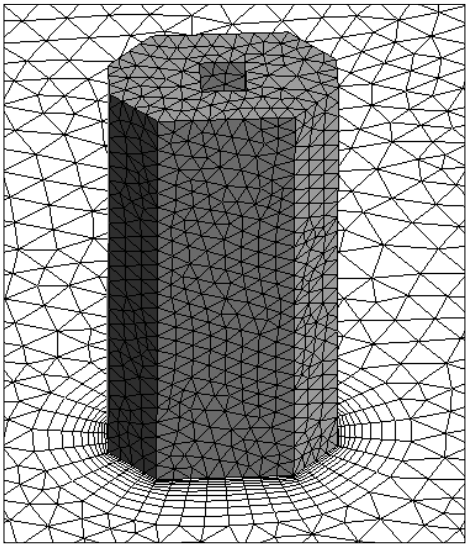

Figure 6. Meshing

7. Computational Grid, Boundary Conditions

The result of the simulation depends significantly on the discretized grid of the computational domain and the model. The resolution of the grid is specified to capture important physical parameters such as pressure on the model surface, vortices created, separation and reattachment of the flow etc. to a precise extent. The discretization of geometry of the model is kept finer than that of the computational grid. Greater the number of cells, better the CFD results. But, increase in number of cells increases the calculation time and also enhanced computing resource is required [24]. In the present study, after some trials with the meshing techniques and the boundary conditions, the final meshing was done with automatic method having element size 90 mm for the domain volume, 40 mm for the ground surface and 20 mm for the model walls and roof. Smooth inflation for the model is given so that the grid from the domain touches the walls orthogonally for smooth transition of simulation on the building surfaces. Meshing is shown in Figure 5. The total no of nodes created are in the order of 465000. The total number of elements are in the order of 2550000. The domain side, top walls and the roof top wall were defined as free slip walls ($\tau_{wall} = 0; u_{wall} = 0$) where τ_{wall} the wall shear stress is and u_{wall} is velocity normal to the wall. Meaning thereby that the velocity component parallel to the wall has a finite value and it is computed during the simulation. But, the velocity normal to the wall and the wall shear stress both are zero. The faces of the model and the ground have been defined as no slip wall ($u_{wall} = 0$) i.e., the velocity of the fluid at wall boundary is zero and there is no wall velocity. For the oblique wind flow, the model is rotated rather than rotating the flow field, the boundary and flow parameters being the same. For 0° wind incident angle the solution was achieved at 108 Nos of iterations probably due to aerodynamic complied octagonal oval-shaped model. The simulation graph for momentum and mass and, that for turbulent kinetic energy and its dissipation are presented in Figures 6(a) and 6(b) respectively for perusal.

8. Result and Discussion

8.1. Flow Characteristics

As wind impinges on upwind surface of the model, airflow separates at the edges of the face and generates recirculation zones over side surfaces, roof and downwind surfaces extending into downwind wake.

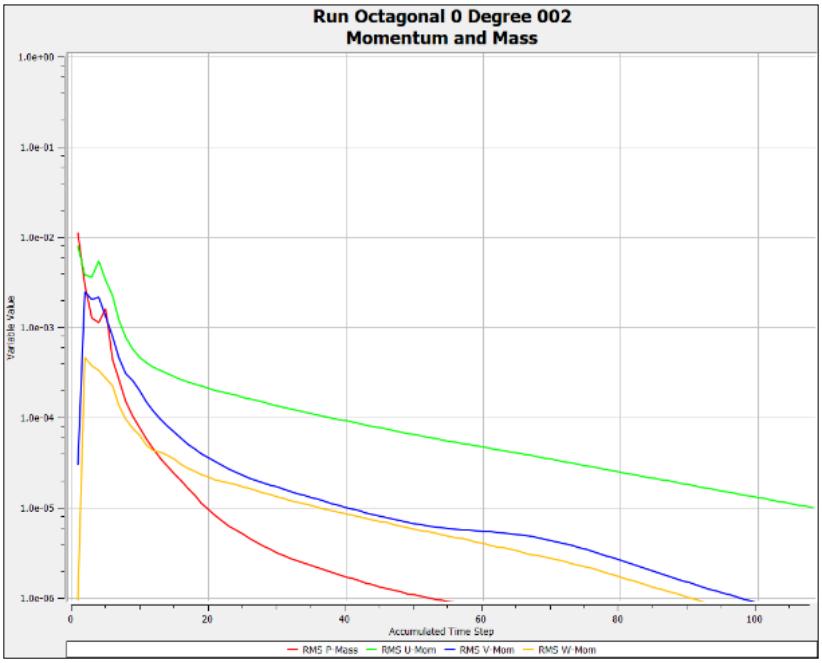

Figure 7 (a). Convergence of Moment and Mass

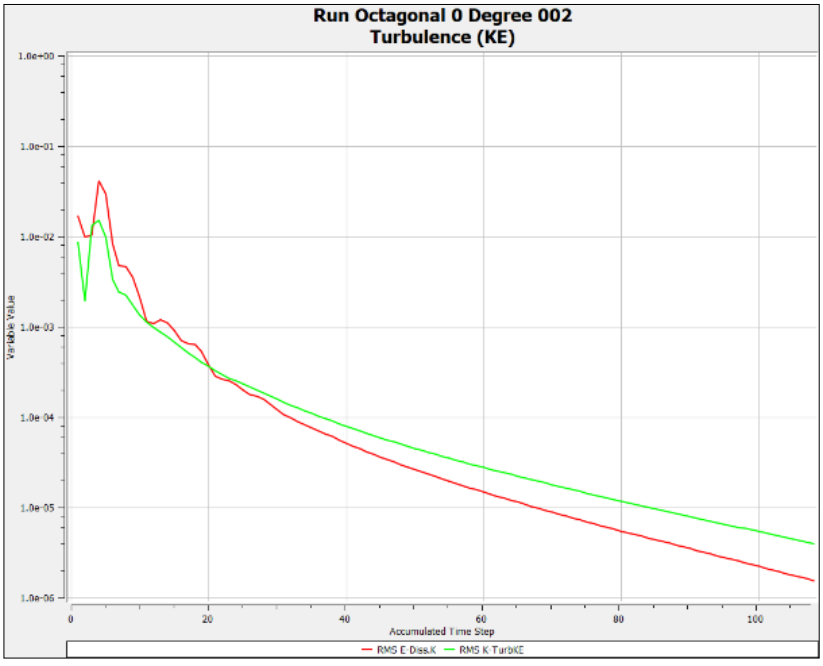

Figure 7 (b). Convergence of Turbulent KE

Streamline patterns at height Z 165 mm and Z 335 mm around the model for all the wind angles are shown in Figures 8(a) to 8(d). The streamline patterns are different for different wind angles. To understand the flow characteristics thoroughly let us discuss the flow pattern for 0° wind incident angle. A typical diagram of flow separation and recirculation at 0° wind incident angles is shown in Figure 9 and that of the wind flow pattern striking on windward face at 0° wind angle is shown in Figure 10. In Figure 9 it is seen that the size and pattern of flow separation and recirculation on the surfaces which are symmetrical along the flow direction are not similar over the surfaces. It is due to the turbulence or gustiness of the approaching wind and the unsteady three-dimensional character of flow; whereas time averaged steady flow condition has been taken in the study.

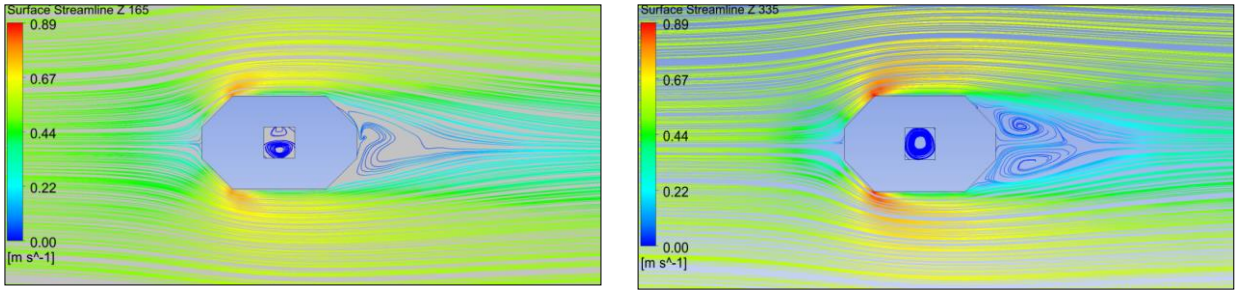

Figure 8 (a). Streamline Pattern at Z 165 and Z 335 at 0° Wind Angle

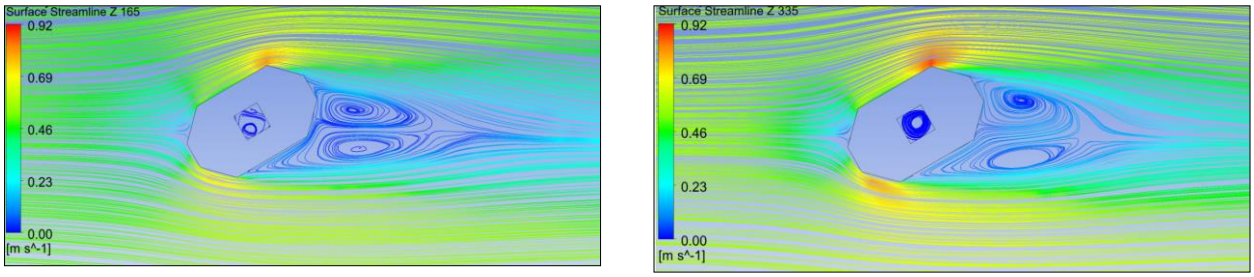

Figure 8 (b). Streamline Pattern at Z 165 and Z 335 at 30° Wind Angle

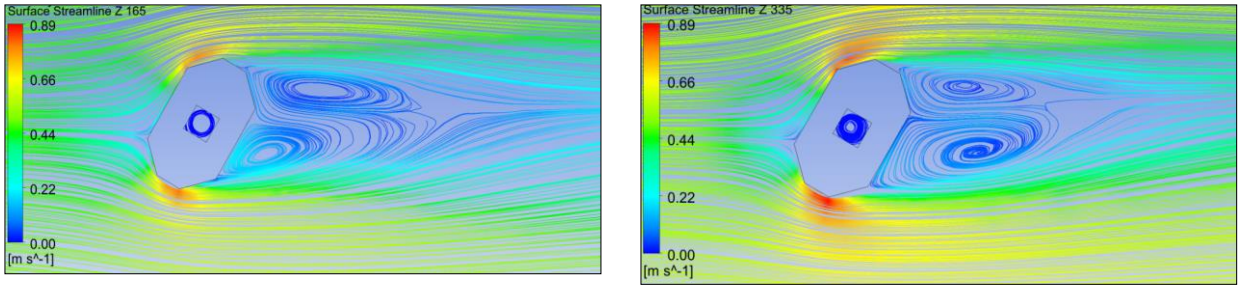

Figure 8 (c). Streamline Pattern at Z 165 and Z 335 at 60° Wind Angle

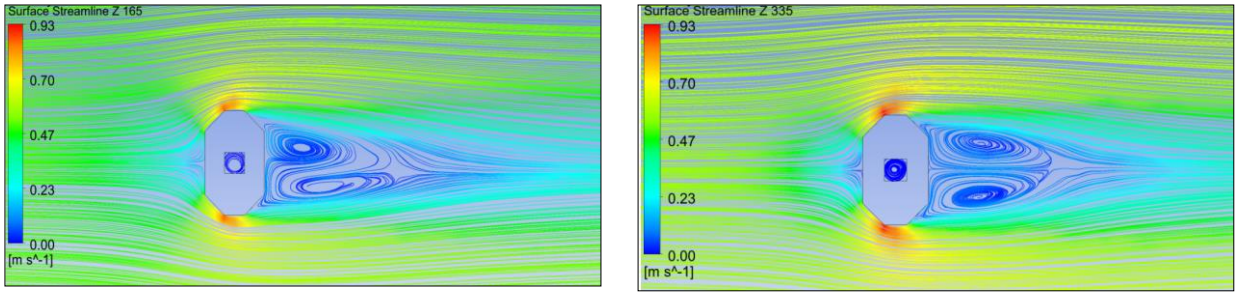

Figure 8 (d). Streamline Pattern at Z 165 and Z 335 at 90° Wind Angle

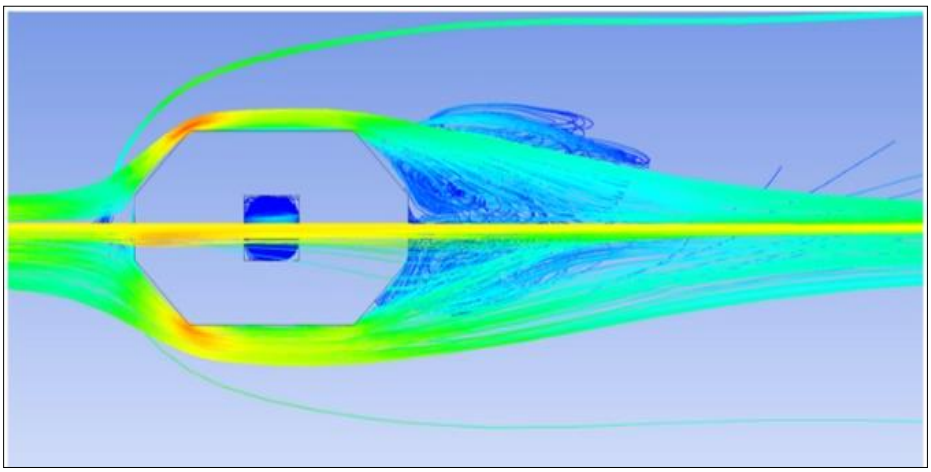

Figure 9. Flow Separation and Recirculation 0° Wind Angle

In the ABL condition the mean wind speed approaching the model increases with height above the ground level. As such, the upper part of the upwind face is experiencing higher wind speed than near the ground. As a result of this, a downwash on approximately the lower one half of the model is being created (Figure 10). On the upper one quarter (approximately) of the face there is an up wash i.e., wind flow is directed upward over the roof. An intermediate stagnation zone is also observed between up wash and downwash region where surface streamlines are passing horizontally around the building. With the change in incident angle from 0° to 90° this stagnation zone is progressively reducing and it is almost nil at 90° wind angle. This can be seen in the Figure 11 in which streamline along wind direction on a central vertical plane for different angles are shown. Downwash on the lower surface of the upwind face is separating from the model before it reaches the ground level and moves upwind to form a vortex as shown in Figure 10. This is generating high velocity near the ground. This ground level upwind vortex is carried around the sides of the model in U shape. Referring Figure 8 again, the flow is reattaching and generating regions of wake where flow recirculation with high turbulence is created forming two distinct vortices. These vortices are continuously hitting the side and downwind surfaces.

The reattachment of flow and formation of vortices for different wind angles and also along the height are different (Figures 8 and 9). The recirculation with high turbulence in the wake region causes low average velocity on the downwind faces (Figure 12). The pattern of flow separation and the velocity magnitudes for different angle of wind are quite evident from these diagrams. It is seen that the flow is separated from the meeting edge of the slant/inclined side face A1 and near end of side face C on one side and meeting edge of slant/inclined face A2 and near end of face D on another side for 0° wind incident angle and, velocity is maximum at these locations. For 30° wind angle it is at the meeting edges of face C and B2 at one side and face A and A2 on another side. For 60° wind angle flow velocity is maximum at the edge of face C and B2 on one side and face A and A2 on another side. For 90° wind angle it is at the edge of face B2 and B on one side and edge A1 and A on another side. Referring Figure 11, it is seen that an upward flow exists over most part of the downwind faces for the respective wind directions. Inside the central opening the surface pressure is suction (negative pressure) throughout the height of the model and is almost same on all the four faces up to the height of about 0.35 m of the model. Again, after about 0.45 m height of the model to the roof top this change is noticeably large. The face, orthogonal to the wind flow and facing the upwind direction experiences higher suction pressure. The face, orthogonal to wind flow but facing the down wind direction suction reduces considerably at the top. It can be observed in Figures 16(a) and 16(d). This may be attributed to recirculation cavity and the influence of shear layer created by the separating wind at the roof top of the central opening. It is more or less similar for all wind angles but, at 90° wind angle this recirculation cavity is projecting above the roof considerably (Figure 11) suggesting high turbulence and creation of vortex resembling S shape. As such, it is important to design the cladding units in this height properly.

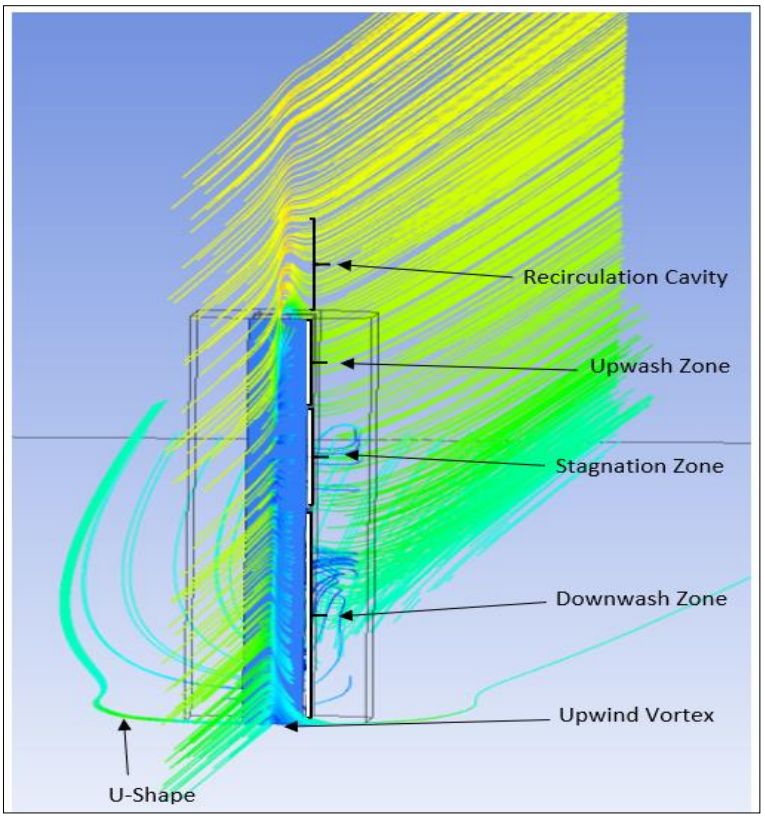

Figure 10. Flow Pattern at 0^0 Wind Angle

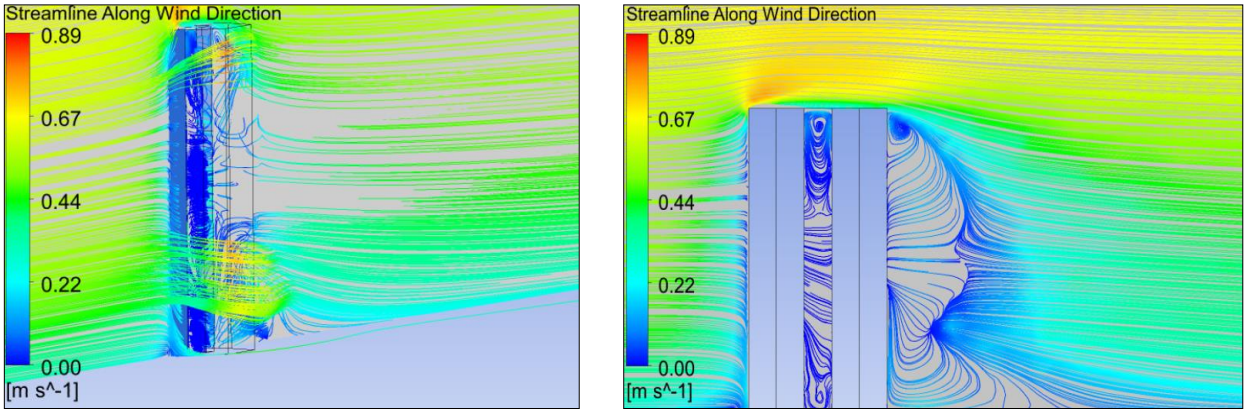

(a): 0° Wind Angle

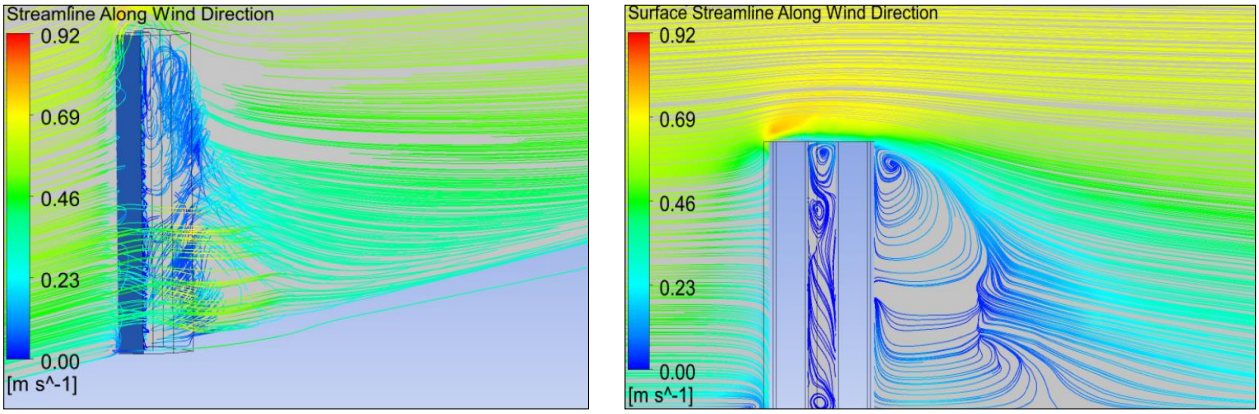

(b): 30° Wind Angle

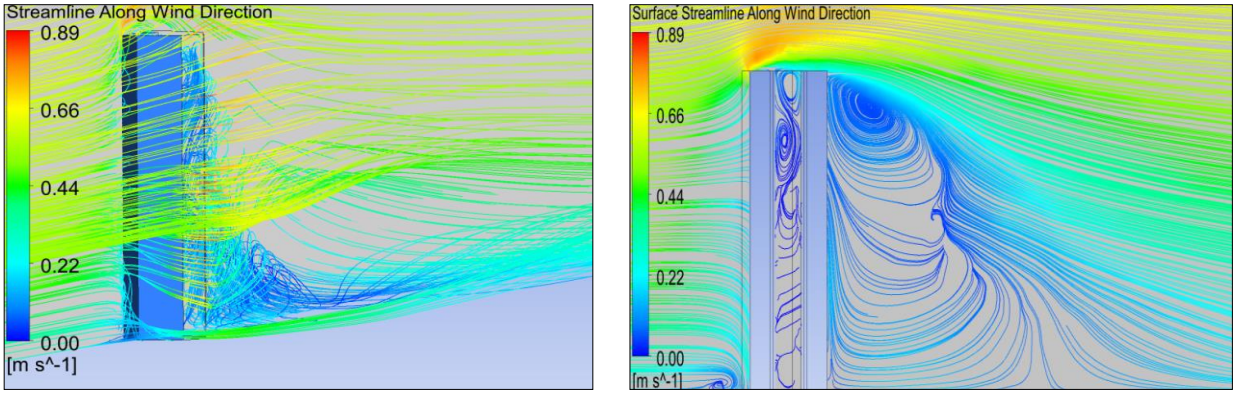

(c): 60° Wind Angle

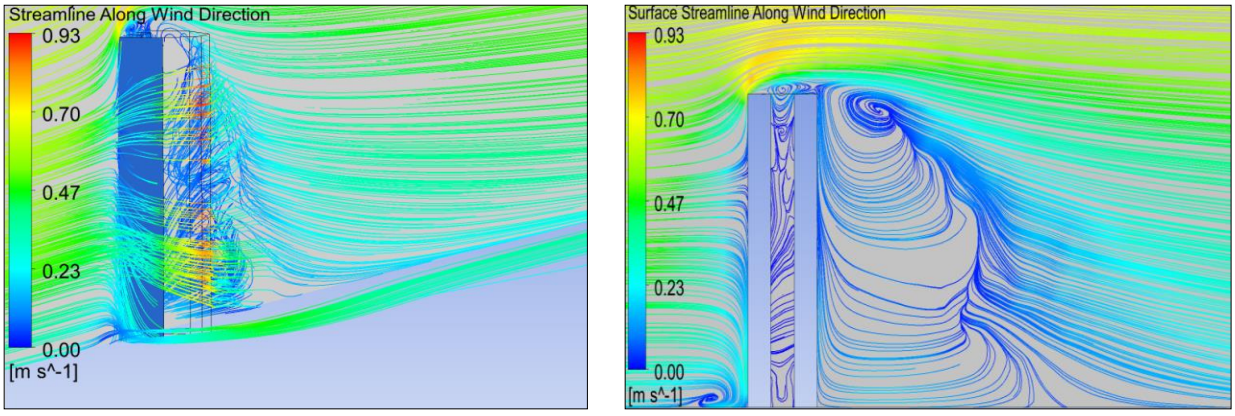

(d): 90° Wind Angle

Figure 11. Streamline Along Central Vertical Plane

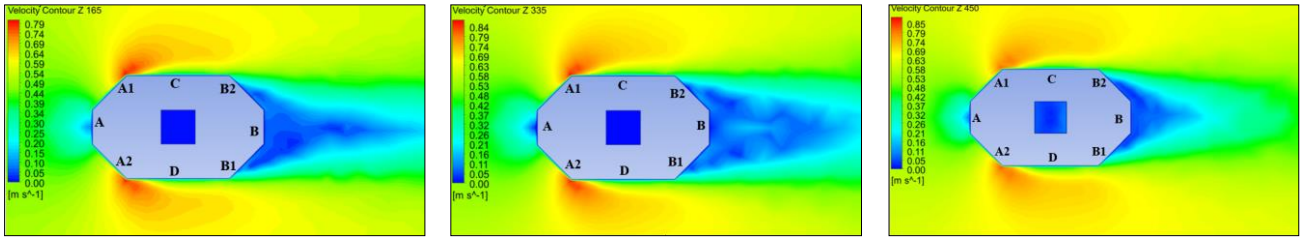

(a): 0° Wind Angles

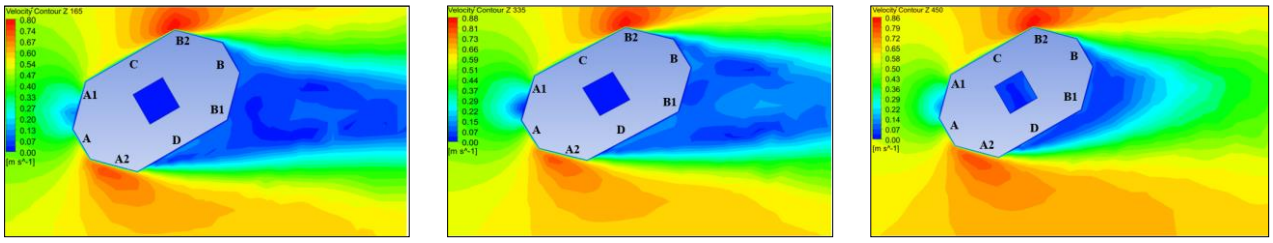

(b): 30° Wind Angles

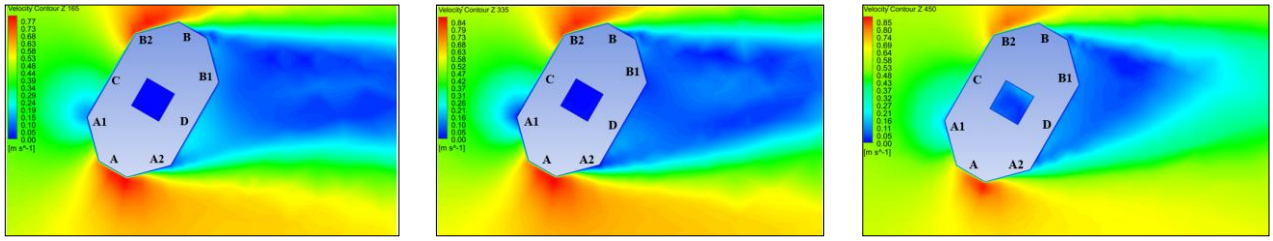

(c): 60° Wind Angles

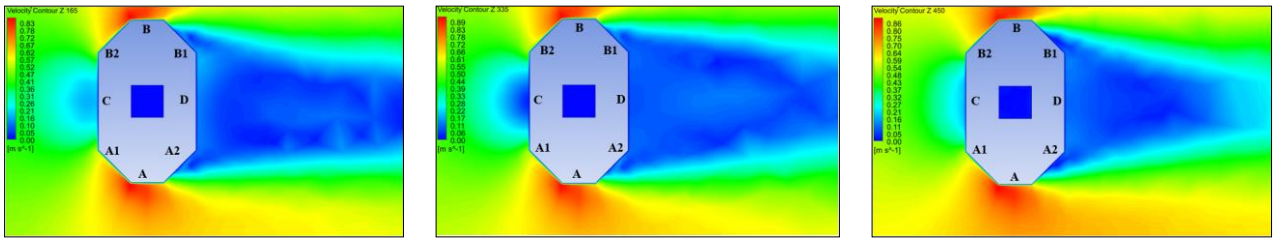

(d): 90° Wind Angles

Figure 12. Velocity Magnitude at Z 165, Z 335 & Z 450

8.2. Pressure/ Pressure Coefficient

The variation of face averaged value of surface pressure coefficients (C_{Pe}) for different faces of the model from 0° to 90° @ 30° wind angle are presented in Figure 13. It is clear from the figure that positive pressure decreases with the increase of wind incident angles on the upwind face A. Negative pressure is experienced on this face when wind incident angle becomes around more than 33°. Mean C_{Pe} on this face varies between +0.68 and -1.40. The C_{Pe} values on faces of the model for different wind angles have been shown in Figures 14(a) to 14(d). Positive C_{Pe} at the windward faces is due to wind energy dissipation and drag force by the incident wind, whereas negative C_{Pe} at the leeward faces is due to vortex generation & backwash. The side faces are subjected to negative C_{Pe} due to uplift force and the side wash. Either positive or negative C_{Pe} on inclined faces exists depending upon their orientation with the direction of flow. Referring to Figure 14 (a), face A, being the windward face, is subjected to maximum positive C_{Pe}. It is more pronounced in the upper middle level of the face and centered from the edges due to greater drag force. The pattern of the C_{Pe} contour is symmetrical about the vertical axis as the wind is impinging perpendicularly on the face. It is also seen that the C_{Pe} contour of higher magnitude exists along the height due to increase in impact pressure as discussed earlier (ABL condition). At the roof level it becomes negative due to uplift force and separation of flow. The slant/inclined upwind faces A1 and A2 are experiencing positive pressure at the near end and progressively reducing to negative towards the far end as the wind accelerates and reaches maximum velocity at the far end of these faces.

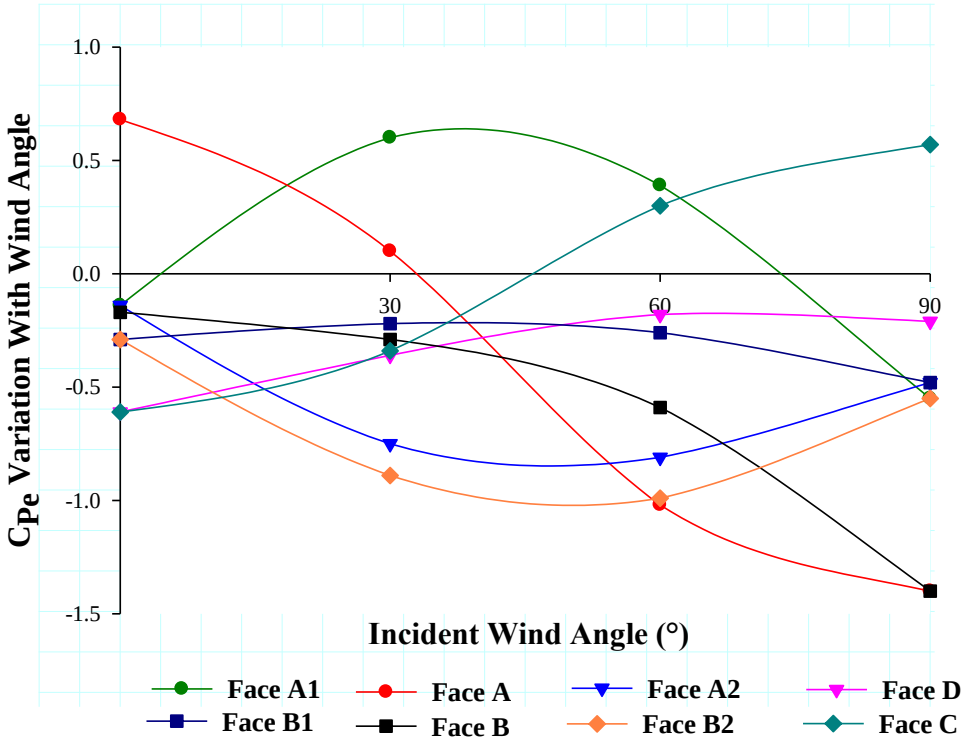

Figure 13. Variation of C_{Pe} With Wind Angle

Though, the faces are symmetrical for this direction of wind (0°), the pressure on faces are not identical as recirculation of flow is not constant over the surfaces due to unsymmetrical flow around the three-dimensional model and local turbulences and eddies. Face C & D being the side faces are subjected to negative pressure due to flow separation from the edges of faces A1 and A2 respectively. The negative pressure on these faces increases from the near end junction of the inclined upwind faces A1 and A2 respectively towards the far end of the respective faces. At the near end the pattern of thermal diagram (blue colour) of C_{Pe} contours on Face C and D suggests high turbulence and creation of local micro level vortices there. The variation of C_{Pe} along the central vertical lines on faces C & D are almost similar, Figure 15 (a). Face B being the downwind face, is subjected to suction pressure due to creation of vortex in the wake region and the back wash. The suction pressure is increasing along the height of face B due to generation of greater uplift force from the backwash created by the vortex. The inclined downwind faces B1 and B2 are facing suction pressure due to backwash and creation of vortices. The suction pressure is decreasing from the edge of face B towards the edges of side faces C & D respectively. With the change in wind direction different faces change their orientation with respect to the direction of impinging wind experiencing different pressure on the same logic explained above. The thermal images of C_{Pe} contours as obtained from post-CFX for different angles of wind have been shown in Figures 14(a) to 14(d).

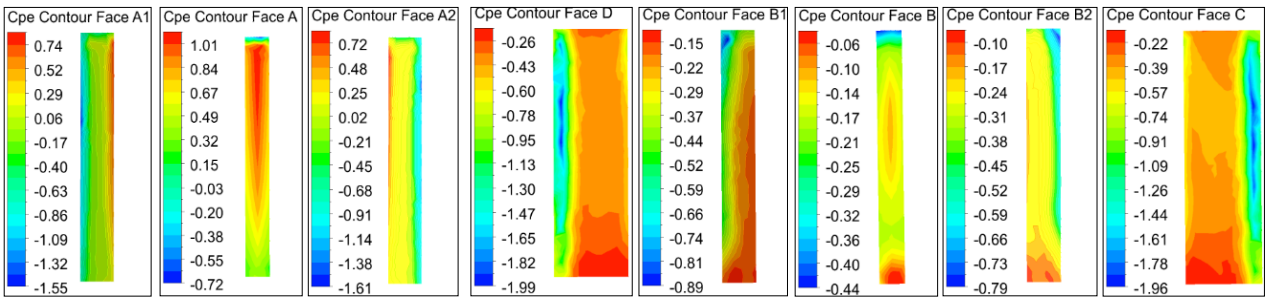

Figure 14 (a). C_{Pe} Contour on Faces 0° Wind Angle

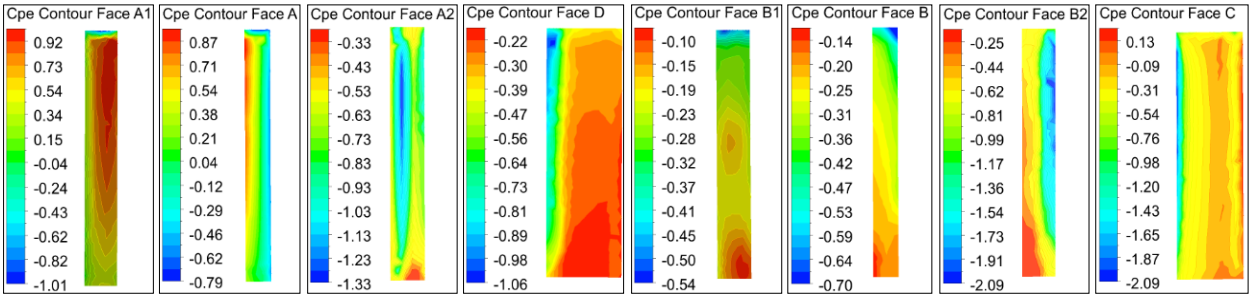

Figure 14 (b): C_{Pe} Contour on Faces 30° Wind Angle

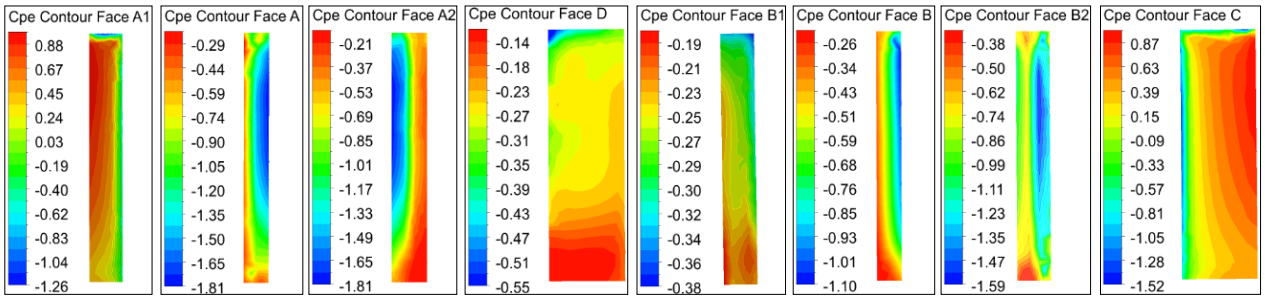

Figure 14 (c). C_{Pe} Contour on Faces 60° Wind Angle

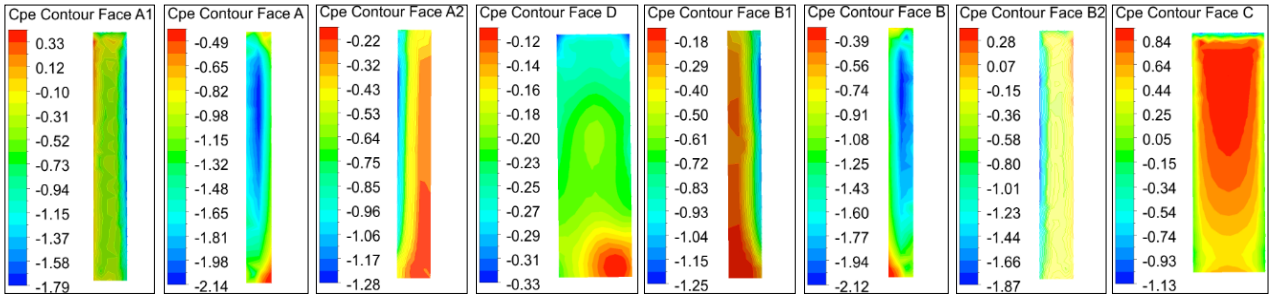

Figure 14 (d): C_{Pe} Contour on Faces 90° Wind Angle

8.3. Central Vertical Pressure Coefficient on Faces

The central vertical C_{Pe} on faces of the model are shown in Figures 15(a) to 15(d). The faces on which the flow is impinging perpendicularly are having positive value of C_{Pe} along the central vertical line. At 0° wind angle upwind face (face A) is having maximum positive C_{Pe} values along the central vertical line compared to that for other wind angles. Maximum positive C_{Pe} (1.25) is at height 0.45 m (95 %) at vertical center line on the face (Figure 15(a)). At 30° wind incident angle almost 1/3rd value (0.4) is noticed at the same location. The inclined upwind faces A1 and A2 are having negative value of C_{Pe} close to zero throughout the height but suddenly grows to sharp positive value due to greater uplift force at that height and again drastically to negative due to flow separation at roof level which reduces the pressure value. Other faces are having almost constant negative values along their respective heights. Some local fluctuations in C_{Pe} line is observed due to unsymmetrical flow pattern around the three-dimensional model and the effect of upwash, downwash and stagnation zones on the upwind face.

At 30° wind angle the fluctuations in values along the central vertical line on face B2 is more pronounced seemingly due to turbulence of flow created by the reattachment of flow on face B2 as well as the recirculation of flow by the downwind vortex. At 60^0 wind angle the central vertical C_{Pe} value on faces C and A1 are positive throughout having sharp changes to negative nearer to the roof height due to flow separation at roof. All other faces are having negative C_{Pe} values. Local fluctuations are seen on face A2 due to reasons explained above. At 90^0 wind angle the central vertical C_{Pe} on upwind face C is positive and on other faces it is negative. Effect of local eddies is seen on the downwind inclined faces A1 and B2 on which C_{Pe} values are fluctuating. On the inner faces the central vertical C_{Pe} is negative in nature and constant on most part of the height for all directions of wind. But it changes its magnitude in between the height from 0.35 to 0.4 m up to the roof for different wind angles. The average central vertical suction C_{Pe} values on the inner faces are progressively increasing as the wind angle increases. The graph of central vertical pressure on inner faces for different wind angles are shown in Figures 16(a) to 16(d).

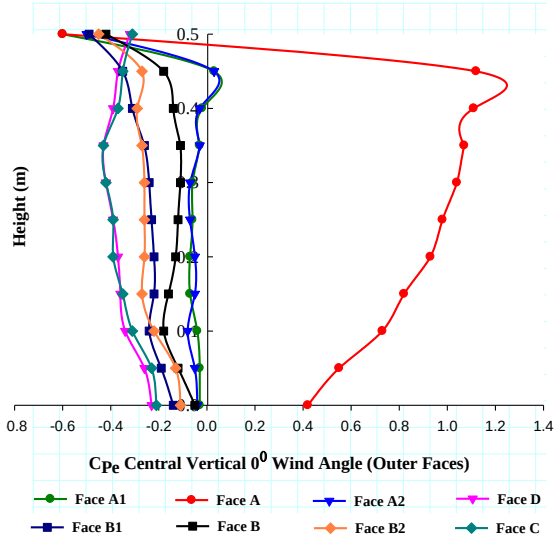

(a). 0° Wind Angle

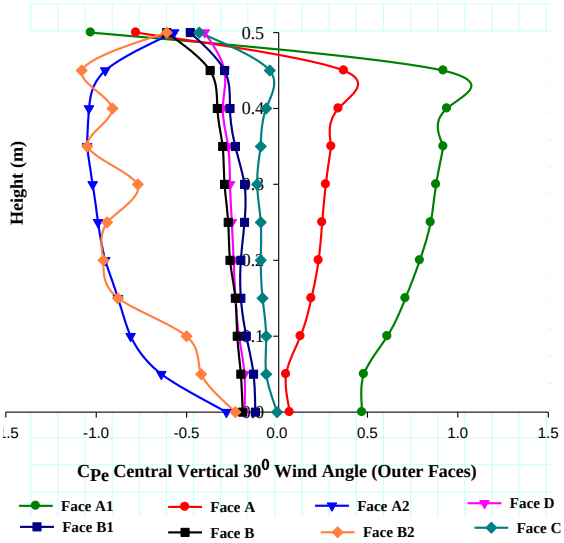

(b). 30° Wind Angle

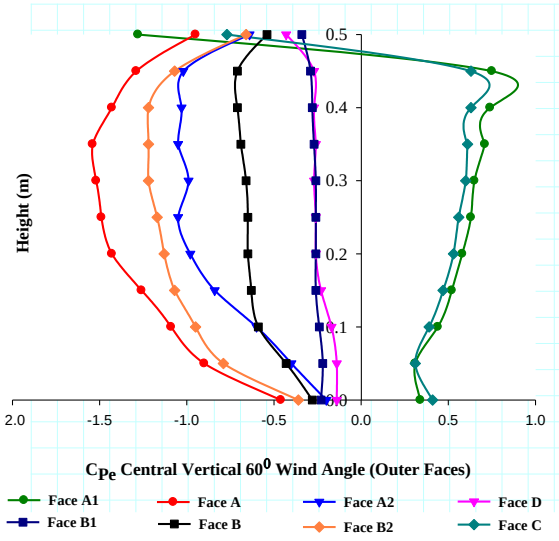

(c): 60° Wind Angle

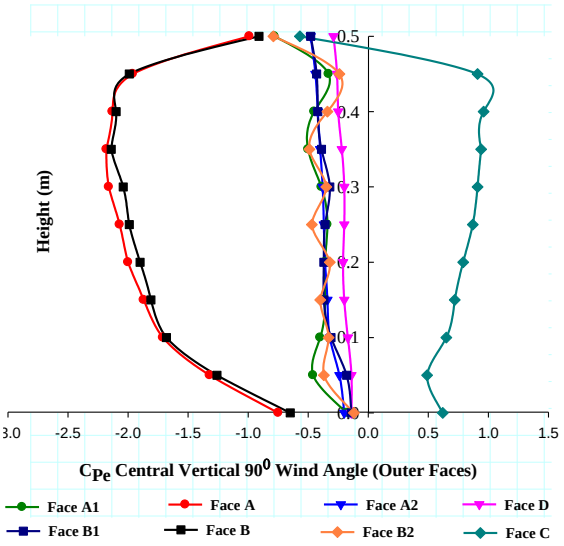

(d): 90° Wind Angle

Figure 15. C_{Pe} Central Vertical on Outer Faces

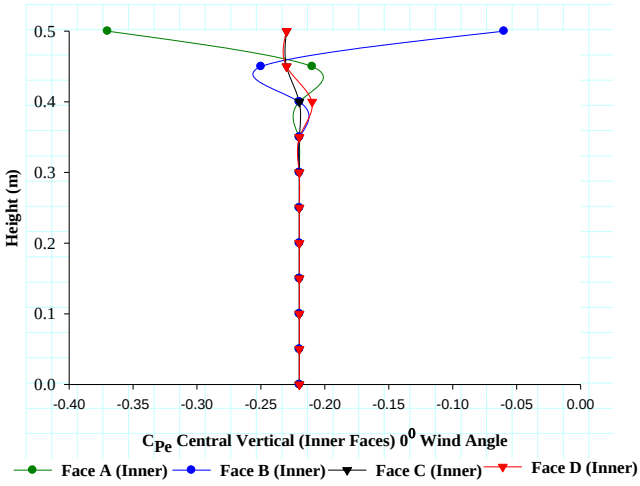

(a): 0° Wind Angle

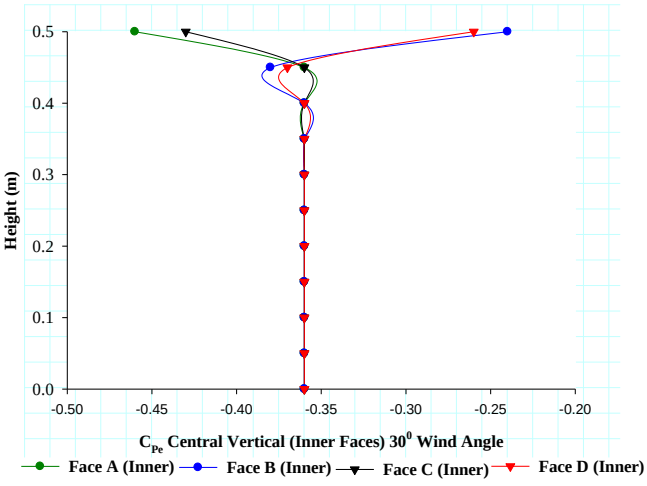

(b): 30° Wind Angle

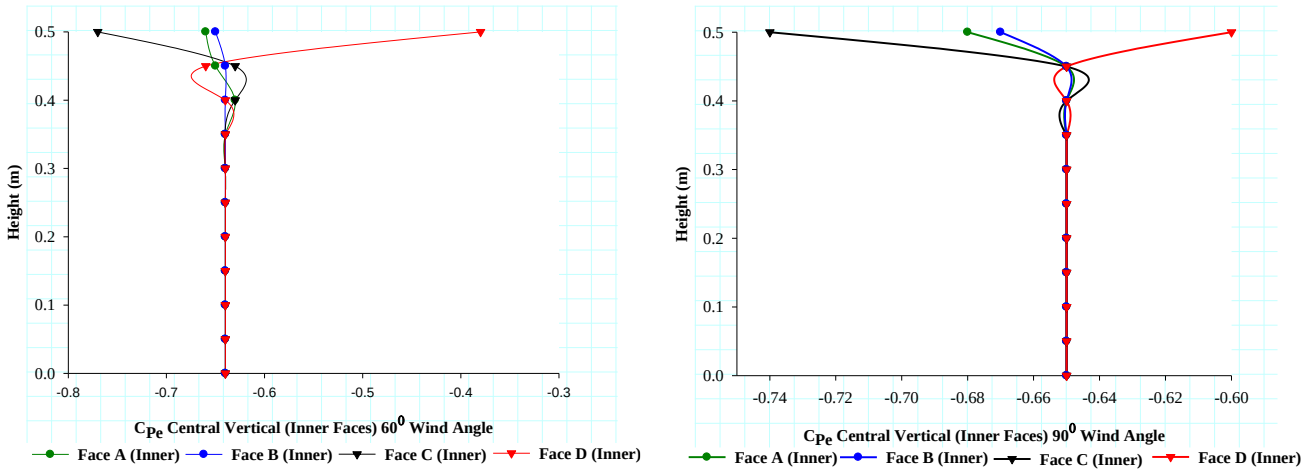

(c): 60° Wind Angle **(d): 90° Wind Angle**

Figure 16. C_{Pe} Central Vertical on Inner Faces

8.4. Pressure Coefficient along Perimeter

The variation of wind pressure coefficients (C_{Pe}) along the perimeter at Z =165 mm and Z = 335 mm height for all the wind incident angles are shown in Figures 17(a) to 17(d). This portrays the overall understanding of the pressure developed on the faces due to different wind angles. Referring to Figure 17 (a), for 0° wind angle, it is seen that the pressure is positive for the entire face of upwind face A and increasing with height. The inclined upwind faces A1 & A2 are facing positive and negative pressure both. The interesting thing is that the for 0° wind angle minimum and maximum C_{Pe} values on these faces are -1.55 & + 0.74 for face A1 and -1.61 & + 0.72 for face A2 respectively, but the face average values are lowest negative (-0.14) for both faces. For 30° wind angle, face A2 is experiencing high fluctuating C_{Pe}. Large variation of C_{Pe} is also observed on face C. This indicated existence of high velocity gradient across the width. The pressure is negative towards the edge B2. It is recovering and becoming positive towards the edge A1. For 60° wind angle face A1 and C are experiencing positive pressure on their major portions. The pressure on face A, A2, B and B2 are though negative but fluctuating across their width. The variation of pressure on face B1 and D are almost nil. For 90° wind angle face C is experiencing positive pressure and rest all other faces are experiencing negative pressure. Face D has very little variation of pressure on its entire face. On face A, A1, B and B2 variation of pressure across their width are large in comparison to A2 and B1.

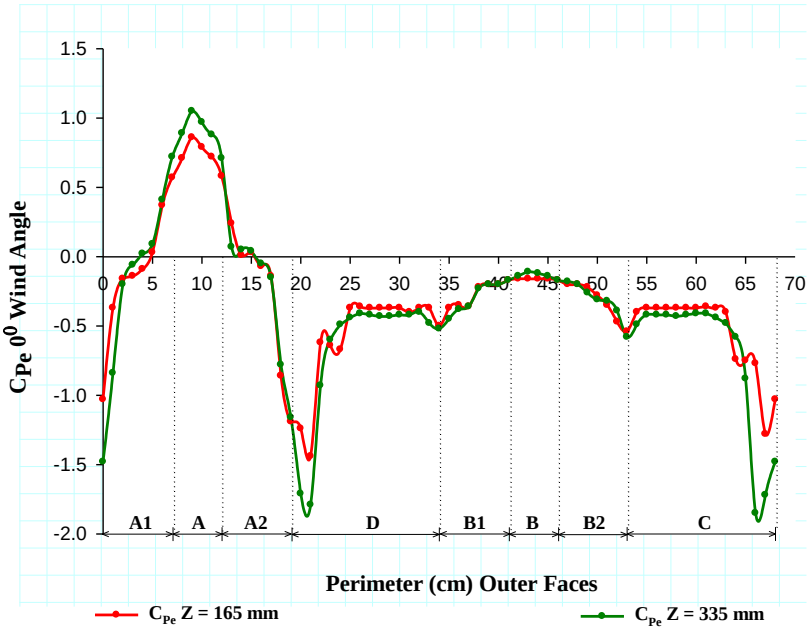

(a): 0° Wind Angle

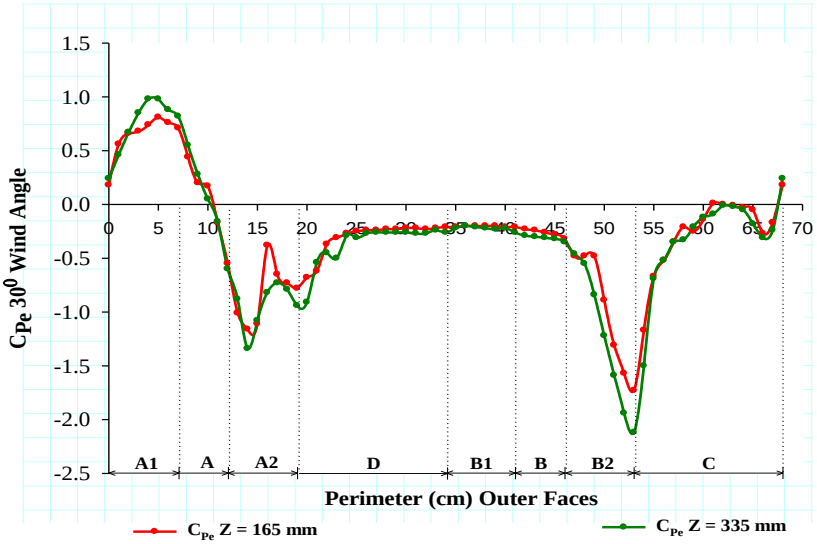

(b): 30° Wind Angle

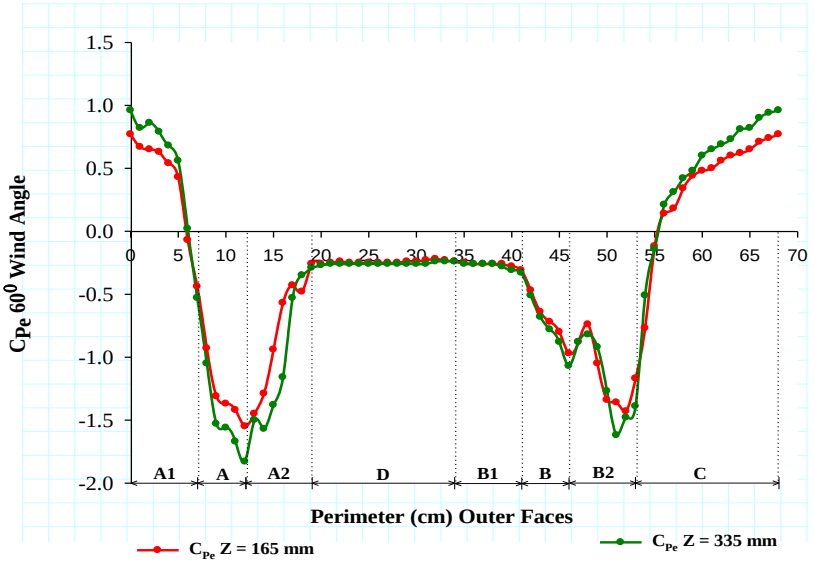

(c): 60° Wind Angle

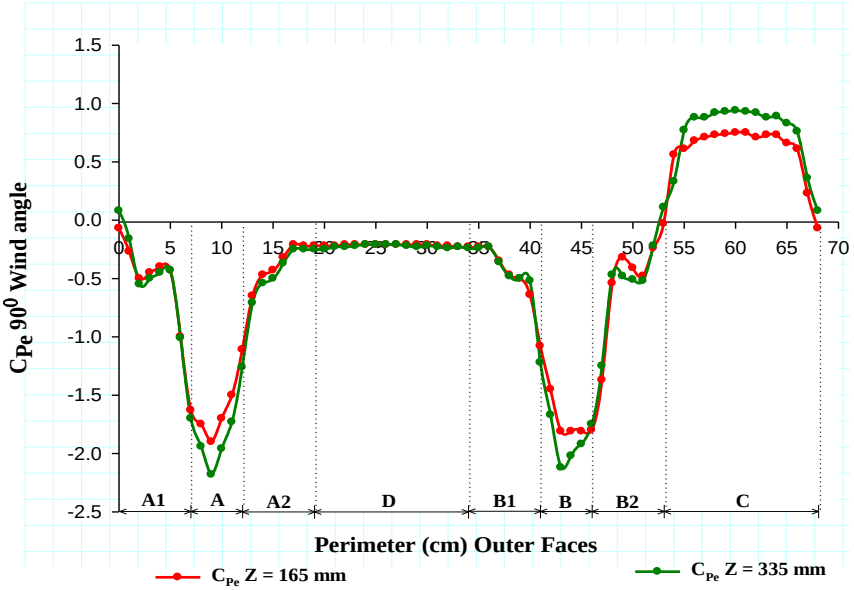

(d): 90° Wind Angle

Figure 17. C_{Pe} Along Perimeter on Faces

9. Conclusions

Natural ventilation in any building improves the air quality, thermal comfort of the inhabitants and reduce energy consumption. Natural cross ventilation is induced by differential pressure difference between different zones of the building.The wind pressure measurements represented herein lead to identification of wind pressure distribution, and hence the pressure differential zones, of an irregular octagonal plan oval-shape building having a central opening and is summarized below.

- For all wind directions the central opening is subjected to negative pressure (suction). It is almost constant for most part of the height of the faces but suddenly reduces in between 0.35 to 0.4 m height of the model due to recirculation cavity and shear layer created by high turbulence. This way it is behaving as a vertical duct for air flow. More sunlight is supposed to enter within the building due to this opening.
- The gradient of pressure across the width on the inclined surfaces for all the wind angles are more pronounced than on the other faces.
- The length/width (side ratio) influences the formation of upwash, downwash and stagnation zone on the upwind faces. The phenomenon widely influences the flow characteristics around the model.
- The ground level upwind vortex which is carried around the model is responsible for deposition of dust and debris close to the ground level, thus contaminating the air environment.
- While the average pressure distribution on the faces (windward, leeward and side faces) are the key to find out the stresses on the structure for structural design, pressure distribution on the faces can be used in better natural ventilation and lighting planning by the architects in the prototype building. Natural ventilation in any building depends upon the wind pressure difference between the openings. Higher the pressure difference, better the ventilation.
- The results presented in this paper for irregular orthogonal plan shape building can be used by the Structural Designers for designing buildings of similar shape for wind loads at any part of the world. Since these coefficients are unitless, no modifications are needed. The only requirement is that the proposed building should have similar height to width ratio and length to width ratio.
- Further study for different irregular octagonal plan oval-shaped buildings with varying height, but with same total floor area may be taken up to optimize the natural ventilation and lighting in such buildings.
- The results of numerical simulation are of great importance at the preliminary stage of project. The exact numerical model for the wind, actually occurring in nature, has not yet been developed by the researchers. However, the results can be relied upon to a greater extent.

10. Declarations

10.1. Author Contributions

Conceptualization, R.R.; methodology, R.R. and A.K.; software, A.K.; validation, A.K. and R.R.; formal analysis, A.K.; investigation, R.R. and A.K.; resources, R.R.; data curation, A.K.; writing—original draft preparation, A.K.; writing—review and editing, R.R.; visualization, A.K.; supervision, R.R.; project administration, R.R.; funding acquisition, R.R. and A.K. All authors have read and agreed to the published version of the manuscript.

10.2. Data Availability Statement

The data presented in this study are available in article.

10.3. Funding and Acknowledgements

Authors would like to express their sincere gratitude to Delhi Technological University, Delhi, India for providing funding to conduct the research work.

10.4. Conflicts of Interest

The authors declare no conflict of interest.

11. References

[1] R. K. Pradeep, V. Ehsan, and S. Azadeh, "Computational Fluid Dynamics Approach for High-rise Buildings," Centre for Earthquake Engineering, IIIT Hyderabad, A3C-12, Report No. IIIT/TR/2013/-1, Hyderabad, (2013): 1–9.

[2] W. D. Baines, "Effect of Velocity Distribution on Wind Loads on a Tall Building," (1952).

[3] Gomes, M. Glória, A. Moret Rodrigues, and Pedro Mendes. "Experimental and Numerical Study of Wind Pressures on Irregular-Plan Shapes." Journal of Wind Engineering and Industrial Aerodynamics 93, no. 10 (October 2005): 741–756. doi:10.1016/j.jweia.2005.08.008.

[4] Mohotti, D., P. Mendis, and T. Ngo. "Application of Computational Fluid Dynamics (CFD) in Predicting the Wind Loads on Tall Buildings - A Case study," ." In 23rd Australasian Conference on the Mechanics of Structures and Materials, Byron Bay, Australia (ACMSM23), (December 2014): 1–6.

[5] Zhao, J. G., and Kit Ming Lam. "Interference effects in a group of tall buildings closely arranged in an L-or T-shaped pattern." Wind & structures 11, no. 1 (2008): 1-18.

[6] Amin, JA, and AK Ahuja. "Experimental Study of Wind-Induced Pressures on Buildings of Various Geometries." International Journal of Engineering, Science and Technology 3, no. 5 (August 2, 2011). doi:10.4314/ijest.v3i5.68562.

[7] Tanaka, Hideyuki, Yukio Tamura, Kazuo Ohtake, Masayoshi Nakai, and Yong Chul Kim. "Experimental Investigation of Aerodynamic Forces and Wind Pressures Acting on Tall Buildings with Various Unconventional Configurations." Journal of Wind Engineering and Industrial Aerodynamics 107–108 (August 2012): 179–191. doi:10.1016/j.jweia.2012.04.014.

[8] Amin, J. A., and A. K. Ahuja. "Effects of Side Ratio on Wind-Induced Pressure Distribution on Rectangular Buildings." Journal of Structures 2013 (August 12, 2013): 1–12. doi:10.1155/2013/176739.

[9] Chakraborty, Souvik, and Sujit Kumar Dalui. "Numerical Study of Surface Pressure on Square Plan Shape Tall Building." In Symposium on Sustainable Infrastructure Development (SID), February 8th to 9th, (2013): 252-258.

[10] Bhattacharyya, Biswarup, Sujit K. Dalui, and Ashok K. Ahuja. "Wind induced pressure on 'E'plan shaped tall buildings." Jordan Journal of Civil Engineering 8, no. 2 (2014): 120-134.

[11] Kheyari, Pallab, and Sujit Kumar Dalui. "Estimation of wind load on a tall building under interference effects: a case study." Jordan Journal of Civil Engineering 9, no. 1 (2015): 84–101.

[12] Roy, K., and A. Kumar Bairagi. "Wind pressure and velocity around stepped unsymmetrical plan shape tall building using CFD simulation—A case study." Asian Journal of Civil Engineering (BHRC) 17, no. 8 (2016): 1055-1075.

[13] Mukherjee, A., and A. K. Bairagi. "Wind pressure and velocity pattern around 'N'plan shape tall building—A case study." Asian Journal of Civil Engineering (BHRC) 18, no. 8 (2017): 1241-1258.

[14] Bairagi, Amlan Kumar, and Sujit Kumar Dalui. "Distribution of Wind Pressure around Different Shape Tall Building." Advances in Structures, Systems and Materials (2020): 31–38. doi:10.1007/978-981-15-3254-2_4.

[15] Pal, Supriya, and Ritu Raj. "Evaluation of Wind Induced Interference Effects on Shape Remodeled Tall Buildings." Arabian Journal for Science and Engineering 46, no. 11 (July 2, 2021): 11425–11445. doi:10.1007/s13369-021-05923-x.

[16] Raj, Ritu, and Ashok Kumar Ahuja. "Wind loads on cross shape tall buildings." Journal of Academia and Industrial Research 2, no. 2 (2013): 111-113.

[17] Ritu Raj, Rana T, Anchalia, and Khola U, "Numerical Study of Wind Excited Action on H Plan-Shaped Tall Building," International Journal of Emerging Technologies 11, no. 3, (2020): 591–605.

[18] Pal, Supriya, Ritu Raj, and S Anbukumar. "Comparative Study of Wind Induced Mutual Interference Effects on Square and Fish-Plan Shape Tall Buildings." Sādhanā 46, no. 2 (April 28, 2021): 1-27. doi:10.1007/s12046-021-01592-6.

[19] Nagar, Suresh K., Ritu Raj, and Nirendra Dev. "Experimental study of wind-induced pressures on tall buildings of different shapes." Wind and Structures 31, no. 5 (2020): 441-453. doi:10.12989/was.2020.31.5.431.

[20] Quan, Yong, Jialu Chen, and Ming Gu. "Aerodynamic Interference Effects of a Proposed Taller High‐rise Building on Wind Pressures on Existing Tall Buildings." The Structural Design of Tall and Special Buildings 29, no. 4 (January 7, 2020): e1703. doi:10.1002/tal.1703.

[21] ANSYS Inc., "ANSYS CFX-Solver Theory Guide," (2009).

[22] Revuz, J., D.M. Hargreaves, and J.S. Owen. "On the Domain Size for the Steady-State CFD Modelling of a Tall Building." Wind and Structures 15, no. 4 (July 25, 2012): 313–329. doi:10.12989/was.2012.15.4.313.

[23] IS 875 (Part 3), "Design Loads (Other than Earthquake) for Building and Structures - Code of Practice Part 3 Wind Loads (Third Revision)," New Delhi: Bureau of Indian Standards, (2015).

[24] Franke, J. "Impact of wind and storm on city life and built environment," Recommendation on the use of CFD in Wind Engineering. In: COST action C14, vol. Version 1.0, (2004): 1–12.